Chemical Engineering Journal 166 (2011) 536–543

Contents lists available at ScienceDirect

Chemical Engineering Journal

journal homepage: www.elsevier.com/locate/cej

Experimental and modeling study of the adsorption of single and binary dye solutions with an ion-exchange membrane adsorber

Jordi Labanda [a,*], Josep Sabaté [b], Joan Llorens [a]

[a] Department of Chemical Engineering, University of Barcelona, Martí i Franquès 1, 08028 Barcelona, Spain
[b] Departament d'Enginyeria Agroalimentària i Biotecnologia, Universitat Politècnica de Catalunya, Edifici ESAB, Avinguda del Canal Olímpic s/n, 08860 Castelldefels, Spain

ARTICLE INFO

Article history:
Received 21 July 2010
Received in revised form 3 November 2010
Accepted 3 November 2010

Keywords:
Ion-exchange membrane adsorber
Binary adsorption
Breakthrough curve
Anionic dye
Separation

ABSTRACT

The adsorption of single and binary mixtures of anionic dyes through an ion-exchange membrane adsorber was analyzed experimentally and theoretically. A generalized model to simulate the dynamic adsorption of multi-component mixtures is put forward. The model is based on the continuity equation, which describes the convection flow through the membrane, the axial dispersion and adsorption on the membrane adsorber and the extended Langmuir isotherm, to explain the competitive adsorption between solutes. The experimental breakthrough curves of the two dyes in binary mixtures were simulated with the parameters of the model determined from the experiments of the single dyes. The dyes were separated on the basis of their different adsorption characteristics.

1. Introduction

Adsorption and ion-exchange processes are by far the most widely used techniques for high-resolution separation and analysis of organic molecules. These processes are traditionally carried out in packed beds, in which the pressure drop is generally high and intra-particle diffusion impedes the transport of solute molecules to binding sites within the pores of such media [1–3]. Moreover, the adsorption of large molecules (such as dyes) requires an adsorbent with a major mesoporous fraction to enhance the efficiency of the process [4,5].

Adsorption of single cationic and anionic dyes on activated carbon has been extensively studied, although activated carbons are expensive and not easy to regenerate [5]. Adsorption of single dyes has been analyzed mostly with Langmuir and Freundlich isotherms, whereas extended Langmuir isotherms, based in some cases on the parameters determined for single-dye solutions [6–8], have been used for the adsorption of multicomponent dye mixtures. Nevertheless, other approaches have been used to explain the non-ideal adsorption of binary dye mixtures. Noroozi et al. [7] and Choy et al. [8] observed better fits in the competitive adsorption of binary cationic dye mixtures on activated carbon following the Jain and Snoeyink model, which adds an additional term to the extended Langmuir equation to incorporate the competition between solutes.

This paper describes the retention and separation of organic molecules with an ion-exchange membrane adsorber (membrane chromatography), which is considered as an alternative to conventional resin-based adsorption columns. Membrane chromatography is performed by ion-exchange, affinity, hydrophobic interaction and reversed-phase membrane adsorbers [9–12], and combines the advantages of conventional chromatography columns in terms of separation power and capacity with membrane technology in its mass transfer, high throughput and robustness. As the main advantage is the absence of long diffusive paths, a process performed with membrane adsorbers is faster than one with a traditional column configuration [13]. Ion-exchange membrane adsorbers operate in convective mode, which significantly reduces the diffusion and the pressure drop limitations commonly encountered in column separation processes [14,15].

The dynamic adsorption of a single solute in a membrane adsorber has been modeled by the differential mass balance in a flat sheet of membrane [16–18]. The continuity equation describes the following parameters: (1) the time derivation of solute concentration in the liquid-phase, (2) the axial convective flux, (3) the axial solute dispersion and (4) the solute adsorption/desorption onto the porous surface of the solid-phase as a function of time. Usually, the physical sorption is described by a second-order kinetic reversible process between adsorption and desorption and assumes the energetic homogeneity of the adsorption sites without steric effects. Under steady state conditions, the kinetic equation leads to the Langmuir equilibrium isotherm. Suen and Etzel [16] modified the model with dimensionless parameters to represent the experimental breakthrough curves. More recent models modified the

* Corresponding author. Tel.: +34 934031334; fax: +34 934021291.
E-mail address: jlabanda@ub.edu (J. Labanda).

1385-8947/$ – see front matter © 2010 Elsevier B.V. All rights reserved.
doi:10.1016/j.cej.2010.11.013

Nomenclature

b_i	constant of Langmuir isotherm (L/mol)
c_i	solute concentration in the liquid-phase (mol/L)
c_{ieq}	equilibrium solute concentration in the liquid-phase (mol/L)
c_{si}	adsorbed solute concentration in the solid-phase (mol/L)
c^*_{si}	maximum adsorbed solute concentration in the solid-phase (mol/L)
c_{si_eq}	equilibrium solute concentration in the solid-phase (mol/L)
$c_{si\_eq\_o}$	equilibrium feed solute concentration in the solid-phase (mol/L)
C_i	dimensionless solute concentration in the liquid-phase
C_{ieq}	dimensionless equilibrium solute concentration in the liquid-phase
C_{si}	dimensionless adsorbed solute concentration in the solid-phase
C_{si_eq}	dimensionless equilibrium solute concentration in the solid-phase
D_{Li}	axial dispersion coefficient (m^2/s)
k_{ai}	adsorption rate constant (L/(mol s))
k_{di}	desorption rate constant (1/s)
$K_{ads,i}$	dimensionless adsorption constant
L	membrane thickness (m)
m_i	dimensionless ratio between the equilibrium solute concentration in the solid-phase and the feed solute concentration
p_i	dimensionless ratio between the equilibrium feed solute concentration in the solid-phase and the maximum possible concentration of adsorbed solute in the solid-phase
Pe_i	axial Peclet number
r_i	Dimensionless ratio between adsorption and desorption constants
t	time (s)
$t_{ads,i}$	characteristic time related to adsorption process (s)
$t_{des,i}$	characteristic time related to desorption process (s)
$t_{disp,i}$	characteristic time related to axial dispersion (s)
$t_{process}$	convective time or characteristic time of the process (s)
V	flow velocity (m/s)
Z	axial distance along the membrane (m)

Greek letters

ε	porosity of membrane
μ	viscosity of water (mPa s)
τ	dimensionless time
ζ	dimensionless spatial variable

adsorption isotherm to obtain better correlation between experimental and calculated data. Shi et al. [17] used the Freundlich isotherm to describe the adsorption process, thereby assuming the non-homogeneous adsorption, and Boi et al. [18] assumed that one solute can bind to more than one adsorption site with different mechanisms and used a bi-Langmuir model. The latter model allows the simulation of asymmetric breakthrough curves. More recently, Labanda et al. [19] solved the continuity equation with dimensionless parameters and with the definition of characteristic times that quantify axial convection, axial dispersion and the adsorption and desorption process.

The aim of the present paper is to study the viability of the separation of synthetic binary dye mixtures (Orange-G, Eosin-B and Ponceau-S) with a commercial flat-sheet ion-exchange membrane adsorber. The experimental dynamic adsorption data, represented by the breakthrough curves, are analyzed by the generalized differential mass balance based on the continuity equation and the extended Langmuir isotherm.

2. Theory

A membrane adsorber is a porous support with a mean porous diameter several times higher than that of the solutes. The movement of solutes in a membrane adsorber of surface A, thickness L, and porosity, ε, is described by the differential mass balance of solutes in a slice of membrane. Assuming that the radial diffusion, radial convection and surface diffusion are negligible, and that the viscosity, density and interstitial velocity of solution are constant, the differential mass balance of each solute of a mixture solution in an ion-exchange membrane adsorber is expressed by the following equation with the corresponding initial and boundary conditions:

$$\varepsilon \cdot \frac{\partial c_i}{\partial t} + \varepsilon \cdot v \cdot \frac{\partial c_i}{\partial z} = \varepsilon \cdot D_{Li} \cdot \frac{\partial^2 c_i}{\partial z^2} - (1-\varepsilon) \cdot \frac{\partial c_{si}}{\partial t} \quad (1)$$

$$c_i = 0 \quad \text{at} \quad z \geq 0, \quad t = 0 \quad (2)$$

$$c_{si} = 0 \quad \text{at} \quad z \geq 0, \quad t = 0 \quad (3)$$

$$\varepsilon \cdot v \cdot c_i - \varepsilon \cdot D_{Li} \frac{\partial c_i}{\partial z} = \varepsilon \cdot v \cdot c_{oi} \quad \text{at} \quad z = 0, \quad t > 0 \quad (4)$$

$$\frac{\partial c_i}{\partial z} = 0 \quad \text{at} \quad z = L, \quad t > 0 \quad (5)$$

where z is the axial coordinate, t is the time, c_i is the solute concentration in the liquid-phase, c_{si} is the adsorbed solute concentration in the solid-phase, v is the axial velocity of the liquid-phase and D_{Li} is the axial dispersion coefficient of the solute. Eqs. (1)–(5) are the generalization of a multi-component solution of the models described in Refs. [16,19].

In a previous study, we described the accumulation of a solute in a single solution in the membrane adsorber by the kinetic sorption equation, which was defined by a second-order kinetic reversible process between adsorption and desorption [19]. Now, for a multicomponent solution, the second order kinetic sorption is also assumed and the competitive adsorption between all solutes is taken into account by the following expression:

$$\frac{\partial c_{si}}{\partial t} = k_{ai} \cdot c_i \cdot (c^*_{si} - c_{si}) - k_{di} \cdot \left(1 + \sum_{\substack{j=1 \\ j \neq i}}^{n} \left(\frac{k_{aj}}{k_{dj}} \cdot c_j \right) \right) \cdot c_{si} \quad (6)$$

where c^*_{si} is the maximum adsorbed solute concentration in the solid phase and k_{ai} and k_{di} are the adsorption and desorption rate constants, respectively, and n is the number of solutes. Under steady state conditions, the equilibrium solute concentration in the solid-phase depends on the equilibrium concentration in the liquid-phase of all solutes and can be deduced from Eq. (6) when $(\partial c_{si}/\partial t) = 0$, leading to the extended Langmuir isotherm:

$$c_{si\_eq} = \frac{b_i \cdot c^*_{si} \cdot c_{i\_eq}}{1 + \sum_{j=1}^{n} b_j \cdot c_{j\_eq}} \quad (7)$$

where b_i is the ratio between the adsorption and desorption rate constants of the single solute, $b_i = k_{ai}/k_{di}$. The extended Langmuir equation assumed: a homogeneous surface with respect to the energy of adsorption, no interactions between adsorbed solutes,

Table 1
Dimensionless parameters of the mathematical model.

$Pe_i = \frac{t_{disp,i}}{t_{process}} = \frac{v \cdot L}{D_{Li}}$	Axial Peclet number of the single solute (–)
$K_{ads,i} = \frac{t_{process}}{t_{ads,i}} = \frac{k_{ai} \cdot c_{oi} \cdot L}{v}$	Dimensionless adsorption constant of the single solute (–)
$r_i = \frac{t_{des,i}}{t_{ads,i}} = b_i \cdot c_{oi}$	Ratio between adsorption and desorption constants of the single solute (–)
$c_{si\_eq\_o} = \frac{r_i}{1+r_i} \cdot c^*_{si}$	Equilibrium feed solute concentration in the solid-phase of the solute (mol/L)
$p_i = \frac{r_i}{1+r_i} = \frac{c_{si\_eq\_o}}{c^*_{si}}$	Ratio of equilibrium feed concentration in the solid-phase to maximum adsorbed concentration in the solid-phase of the single solute (–)
$m_i = \frac{1-\varepsilon}{\varepsilon} \cdot \frac{c_{si\_eq\_o}}{c_{oi}} = \frac{1-\varepsilon}{\varepsilon} \cdot \frac{b_i \cdot c^*_{si}}{1+\sum_{j=1}^{n} b_j \cdot c_{oj}}$	Ratio of equilibrium feed concentration in the solid-phase to feed concentration of the single solute (–)

and that all adsorption sites are equally available to all solutes. The kinetic equation can be rewritten using Eq. (7) as:

$$\frac{\partial c_{si}}{\partial t} = \left[b_i \cdot c_i + \left(1 + \sum_{\substack{j=1 \\ j \neq i}}^{n} (b_j \cdot c_{eq,j}) \right) \right] \cdot (c_{si\_eq} - c_{si}) \quad (8)$$

Eqs. (6)–(8) can be simplified for single-solute solutions leading to the model described previously [19].

The total solute mass transfer from the liquid-phase to the solid-phase is controlled by four time-dependent processes, which can be described by their respective characteristic times: the process time that is defined as the average time taken by a liquid element to pass through the membrane, $t_{process} = L/v$, the axial dispersion time of a solute, $t_{disp,i}$, and the adsorption and desorption times of a solute, $t_{ads,i}$ and $t_{des,i}$. The dispersion, adsorption and desorption times are calculated and referred to each solute present in a multi-component solution as follow [19]:

$$t_{disp,i} = \frac{L^2}{D_{Li}} \quad (9)$$

$$t_{ads,i} = \frac{1}{k_{ai} \cdot c_{oi}} \quad (10)$$

$$t_{des,i} = \frac{1}{k_{di}} \quad (11)$$

The comparative importance of the dispersion, adsorption and desorption mechanisms in the process is directly related to their characteristic times measured in terms of process time. If the dispersion, adsorption or desorption time is lower than the process time, $t_{process}$, their corresponding mechanism is significant in the overall process and vice versa. In addition, the differences between characteristic times of the solutes show whether the separation is feasible.

These four characteristic times allow three dimensionless parameters to be defined: the axial Peclet number that relates the convection flux and axial diffusion, Pe_i, dimensionless adsorption constant, $K_{ads,i}$, and r_i that relates the adsorption and desorption kinetic constants. Table 1 shows the expressions of all dimensionless parameters that allow for the rewriting of the differential mass balance and the initial and boundary conditions for a multi-component solution in terms such as [19]:

$$\frac{\partial C_i}{\partial \tau} + \frac{\partial C_i}{\partial \zeta} = \frac{1}{Pe_i} \cdot \frac{\partial^2 C_i}{\partial \zeta^2} - m_i \cdot \frac{\partial C_{si}}{\partial \tau} \quad (12)$$

$$C_i = 0 \quad \text{at} \quad \zeta \geq 0, \quad \tau = 0 \quad (13)$$

$$C_{si} = 0 \quad \text{at} \quad \zeta \geq 0, \quad \tau = 0 \quad (14)$$

$$C_i - \frac{1}{Pe_i} \frac{\partial C_i}{\partial \zeta} = C_{oi} \quad \text{at} \quad \zeta = 0, \quad \tau > 0 \quad (15)$$

$$\frac{\partial C_i}{\partial \zeta} = 0 \quad \text{at} \quad \zeta = 1, \quad \tau > 0 \quad (16)$$

where C_i is the ratio between the punctual and the feed solute concentration in the liquid-phase, $C_i = c_i/c_{oi}$, C_{si} is the ratio between the punctual and the equilibrium feed solute concentration in the solid-phase in equilibrium with c_{oi}, $C_{si} = c_{si}/c_{si\_eq\_o}$, ζ is a dimensionless coordinate along the membrane, $\zeta = z/L$, and τ is a dimensionless time defined as the ratio between the current time and the characteristic time of the process, $\tau = t/t_{process}$. All dimensionless parameters are shown in Table 1.

The kinetic and isotherm equations, Eqs. (2) and (3), can also be rewritten in dimensionless form:

$$\frac{\partial C_{si}}{\partial \tau} = K_{ads,i} \cdot \left(C_i + \frac{1}{r_i} \cdot \left(1 + \sum_{\substack{j=1 \\ j \neq i}}^{n} r_j \cdot C_j \right) \right) \cdot (C_{si\_eq} - C_{si}) \quad (17)$$

$$C_{si\_eq} = \frac{\frac{r_i}{p_i} \cdot C_{i\_eq}}{1 + \sum_{j=1}^{n} r_j \cdot C_{j\_eq}} \quad (18)$$

The model is governed by Eqs. (12), (17) and (18), which were implemented in the program "Mathematica" (Wolfram Research) in order to solve the differentials and to simulate the dynamic adsorption of each solute present in a mixture solution. The model depends on five independent dimensionless parameters for each solute: three of those parameters can be calculated from the adsorption isotherm (r_i, p_i and m_i) and two parameters can be determined from the breakthrough curves (Pe_i and $K_{ads,i}$). The detailed process to determine the values of the model's parameters was discussed in a previous paper [19].

3. Experimental

The adsorption of three anionic dyes (Orange-G, Eosin-B and Ponceau-S), supplied by Sigma–Aldrich (Germany), through a Sartobind ion-exchange membrane adsorber (Sartorius, Germany) was investigated to test the model predictions. The molecular structure of the anionic dye is shown in Fig. 1 and the main physical characteristics of three dyes are shown in Table 2. We selected dyes with different anionic groups to study the adsorption properties of each group: Orange-G and Ponceau-S with ionized sulfonic acid groups (2 and 4, respectively) and Eosin-B with ionized carboxylic and alcoholate acid groups. Orange-G has a pK_a value of 11.5 for the deprotonation of the naphthalene OH and a pK_a lower than 2 for the deprotonation of the $-SO_3H$ acid groups. Therefore, at pH = 7 only the sulfonic acid groups are ionized and the molecule has two negative charges [21,22]. Eosin-B has a pK_a1 of 3.2 for the deprotonation of the anthracene OH acid group and a pK_a2 of 3.8 for the deprotonation of the carboxylic group [23]. Therefore, at pH = 7 the molecule has two negative charges. Fig. 1 shows the ionization of Eosin-B. Ponceau-S only presents strong benzene and naphthalene sulfonic acid groups ($pK_a < 2.1$) and the molecule has four negative charges

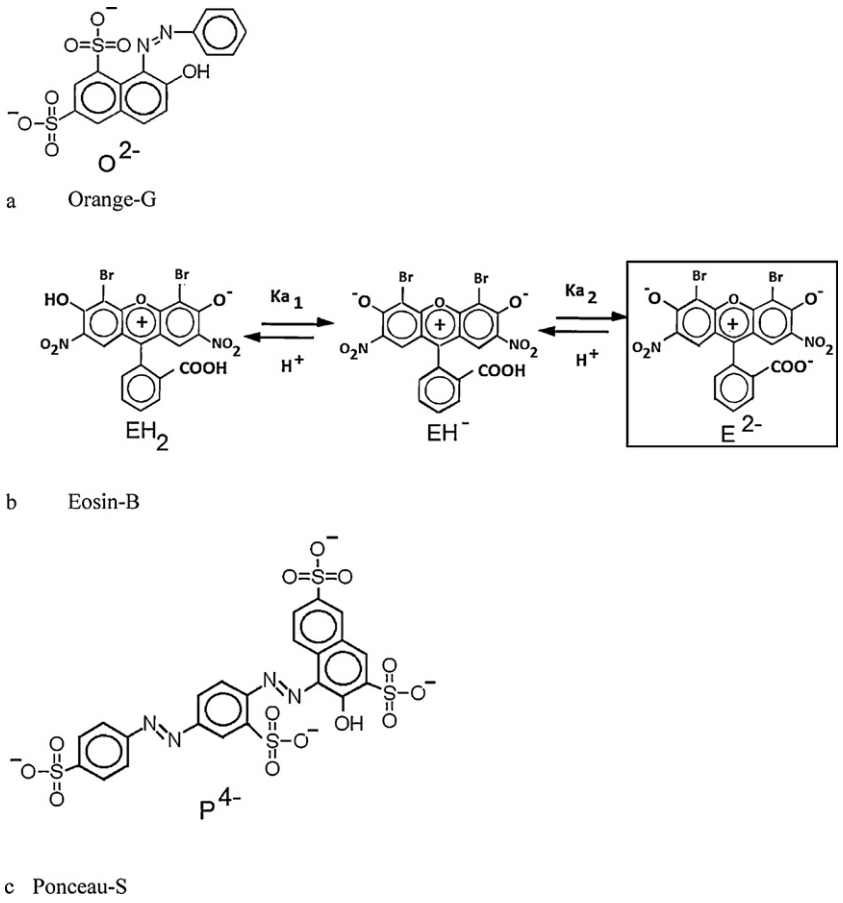

Fig. 1. Chemical structure of the dyes: (a) Orange-G, (b) Eosin-B and (c) Ponceau-S.

at pH = 7. All dyes were at least 95% pure and the initial concentration reported in this study is after adjusting the concentration based on purity. The membrane cartridge is formed by 3 flat-sheets that main features are: 25 mm of diameter (4.91 cm^2 of membrane area), an average membrane thickness of about 0.8 mm and a porosity of 78%. In this study, two membrane adsorbers were used: Sartobind D and Sartobind S with diethylamine and sulfonic functional groups, respectively. The adsorption of anionic dyes was analyzed with Sartobind D; and Sartobind S was only used to conduct non-adsorbing experiments.

The feed solutions were prepared weekly by adding the powder dye to a buffer solution at 0.5 mol/L in KCl and pH = 7, which was fixed by phosphoric buffer. The use of this high KCl concentration was due to the high adsorption observed with Eosin-B and Ponceau-S at lower KCl concentrations. The stack dye solutions were kept in a dark bottle to prevent the color-aging effect. Fig. 2 shows the two experimental configurations used in this study to analyze the adsorption isotherm and dynamic adsorption. Solutions were fed into the membrane cartridge by a single NE-1000 syringe pump (New Era Pump Systems Inc., New York). The dispersion produced in the system device without the membrane adsorber was proved to be irrelevant. The experimental device was placed inside a constant climate chamber to conduct the experiments at a constant temperature of $25 \pm 1\,^{\circ}C$.

Isotherm experiments were conducted by continuously pumping a fixed volume of the feed solution to the membrane cartridge in alternating cycles back and forth in a push–pull action (Fig. 2a), till reaching the equilibrium (48 h). The adsorbed dye concentration was determined by the difference between the initial and final solute concentrations in the liquid-phase. On the other hand, dynamic experiments were performed by continuously pumping the feed solution at a constant flow rate of 1 mL min^{-1} in one direction until completing the breakthrough curves (Fig. 2b). The outlet dye concentrations were determined every 5 mL. Between runs, the adsorbed dye was eluted by a solution of 2 mol/L KCl, and thereafter the membrane adsorber was regenerated with 0.1 mol/L HCl and equilibrated with phosphoric buffer at 0.5 mol/L KCl.

Table 2
Properties of the studied dyes.

Characteristics	Orange-G	Eosin-B	Ponceau-S
Color index number	16,230	45.400	27,195
Molecular weight (g/mol)	452.37	624.08	760.6
Groups	Sulfonic	Carboxylic and anthracene-O^-	Sulfonic
Number of anionic groups	2	2	4
λ_{max} (nm)	478	514	520
Diffusion coefficient[a] (m^2/s)	4.2×10^{-10}	6×10^{-10}	7.1×10^{-10}

[a] The molecular diffusion coefficient of dyes was calculated by the Hayduk and Laudie method [20], where the LaBas molar volume was estimated with Cs Chem3D Ultra® (Molecular Modeling and Analysis).

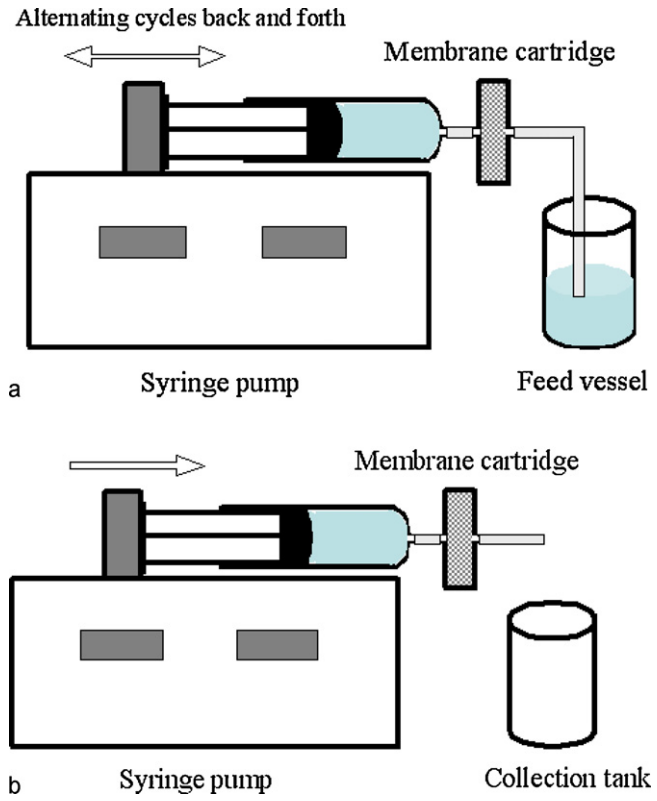

Fig. 2. Diagram of the experimental devices used for (a) equilibrium and (b) dynamic experiments.

Dye concentrations were determined with a UV–visible spectrophotometer (Secoman, France). The dye concentrations in a single solution were calculated from the absorbance, A, measured at the wavelengths showed in Table 2. For binary mixtures, the concentration of both dyes, C_X and C_Y, was correlated with the absorbance measured at the wavelengths of the two dyes, $A_{\lambda 1}$ and $A_{\lambda 2}$, respectively, as follows [24]:

$$C_X = \frac{F_{Y2} \cdot A_{\lambda 1} - F_{Y1} \cdot A_{\lambda 2}}{F_{X1} \cdot F_{Y2} - F_{X2} \cdot F_{Y1}} \quad (19)$$

$$C_Y = \frac{F_{X1} \cdot A_{\lambda 2} - F_{X2} \cdot A_{\lambda 1}}{F_{X1} \cdot F_{Y2} - F_{X2} \cdot F_{Y1}} \quad (20)$$

where F_{X1}, F_{Y1}, F_{X2} and F_{Y2} are the calibration constants for the two dyes.

4. Results and discussion

4.1. Adsorption of single solutes

4.1.1. Equilibrium adsorption isotherms

The equilibrium adsorption isotherms of three dyes are shown in Fig. 3. The Langmuir equation (Eq. (7)) correlated strongly with the experimental data. Each dye showed different adsorption capabilities due to differences in molecular dye characteristics. For instance, when equilibrium concentration in the liquid-phase was 10^{-4} mol/L, the adsorbed concentrations in the solid-phase were 0.00426, 0.0763 and 0.109 mol/L for Orange-G, Eosin-B and Ponceau-S, respectively. The parameters c_s^* and b of the Langmuir isotherm were obtained by minimizing the sum of squares of error, SSE, between the experimental and calculated data. The good fit of the experimental points to the Langmuir isotherm makes it reasonable to assume monolayer adsorption. Table 3 shows the parameters calculated with an SSE lower than 10^{-4}. Affinity (quantified by the parameter b) and maximum adsorption depended on the molecular dye structure. As a first approximation, both parameters increase with molecular size and with the number of anionic groups. Ponceau-S, which has the highest molecular weight and four anionic groups, shows the greatest affinity. Its isotherm rises sharply to the highest maximum adsorption at the lowest bulk dye concentration. The lower adsorption of Orange-G, which is corroborated with the dynamic measurements, as it will be discussed later, corresponds to a low number of anionic groups (two vs. four for the Ponceau-S). While the adsorption capacity of Eosine-B is slightly lower than the Ponceau-S but higher than the Orange-G. Taking into account the electric charge of Eosine-B, the adsorption capacity of this dye would be similar to the Orange-G and lower than Ponceau-S, but the extra hydrophobic adsorption, due to the anthracene part in the dye, counteracts the lower charge opposite

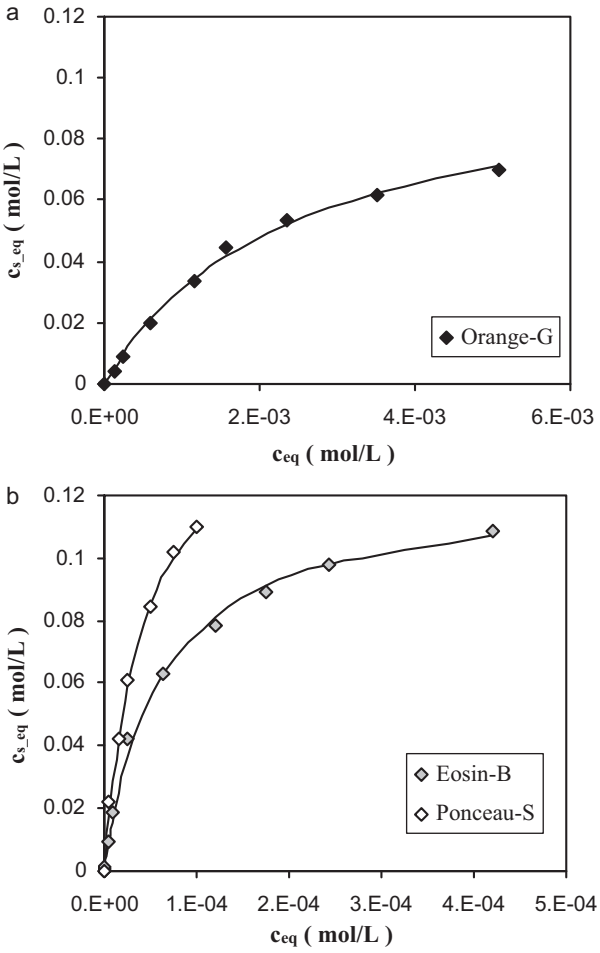

Fig. 3. Equilibrium adsorption isotherms of single dye solutions: (a) Orange-G, (b) Eosin-B and Ponceau-S.

Table 3
Parameters of the model obtained in the simulation of the experimental data. The parameters c_s^* and b were obtained from equilibrium data and the characteristics time from dynamic experiments ($t_{process}$ = 23.6 s).

Parameters	Dye name		
	Orange-G	Eosin-B	Ponceau-S
c_s^* (mol/L)	0.104	0.122	0.152
b (L/mol)	429	16,612	25,240
t_{disp} (s)	49.5	49.5	49.5
t_{ads} (s)	33.7	23.6	18.2
t_{des} (s)	3.62	86.3	91.9

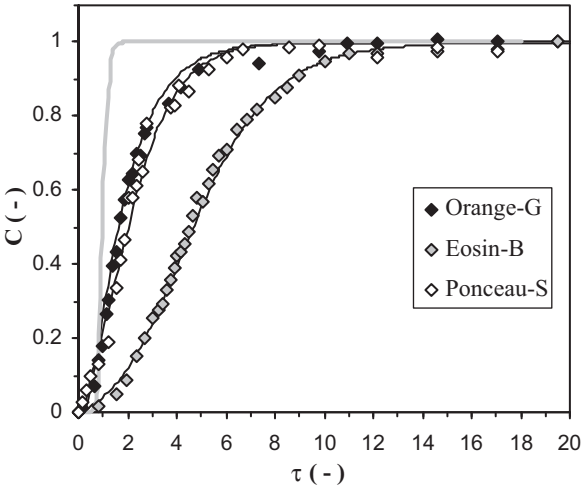

Fig. 4. Experimental and calculated breakthrough curves under non-adsorbing conditions with a cationic membrane adsorber (Sartobind S). The gray line corresponds to a simulated breakthrough curve with the molecular diffusivity coefficient.

to that of Ponceau-S. The maximum adsorption concentration for Ponceau-S was not achieved due to their high adsorption capability, which could complicate the regeneration process of the membrane. However, the maximum concentration of Ponceau-S used in the dynamic experiments (10^{-4} mol/L) is included in the isotherm.

4.1.2. Dispersion experiments (Peclet number)

The dispersion of a dye molecule depends on its diffusion coefficient and the physical characteristics of the porous media. The morphology of Sartobind membranes was analyzed by SEM images [25]. As it was demonstrated that these membranes have an anisotropic macroporous structure, the diffusivity coefficient was expected to be smaller than the axial dispersion coefficient caused by hydrodynamic flow. Dispersion in a regular capillary tube behaves very differently from that in a disordered porous medium [26].

The axial dispersion coefficient was determined experimentally under non-adsorbing conditions. Thus, the Peclet number was decoupled from the dimensionless adsorption constant. The Peclet number was determined with the breakthrough curve under non-adsorbing conditions using the experimental device shown in Fig. 2b. The non-adsorbing conditions were obtained by conducting the experiments with a strongly acid cation exchange membrane adsorber with sulfonic groups (Sartobind S). The anionic groups of dye molecules cannot interact electrically with the sulfonic groups of the membrane adsorber.

Fig. 4 shows the breakthrough curves of the three dyes obtained with the sulfonic membrane adsorber. The gray line corresponds to a simulated breakthrough curve with the Peclet number calculated with the diffusivity coefficient. This breakthrough curve shows an abrupt increase in concentration. However, the breakthrough curves of the three dyes were smoother and displaced to higher dimensionless time. This change in the breakthrough curve's shape means that the dispersion coefficient of dyes is higher than the molecular diffusivity coefficient; thus, the displacement of the breakthrough curves is probably due to residual adsorption, which is difficult to completely avoid. Under ideal non-adsorption conditions, the outlet dimensionless dye concentration of 0.5 is detected at dimensionless time equal to 1. In contrast, this concentration was obtained at dimensionless time equal to 1.65, 1.9 and 4.6 for Orange-G, Eosin-B and Ponceau-S, respectively, thereby indicating the presence of some adsorption mechanism different from electrostatic interaction, especially for Eosin-B. Hydrophobic adsorption, which takes into account interactions between benzene, naphthalene and anthracene groups of the dye's molecular structure. In fact, as can be seen in Fig. 4, Eosin-B showed the highest non-electrostatic adsorption probably as a result of its higher hydrophobicity due to anthracene part in their molecular structure.

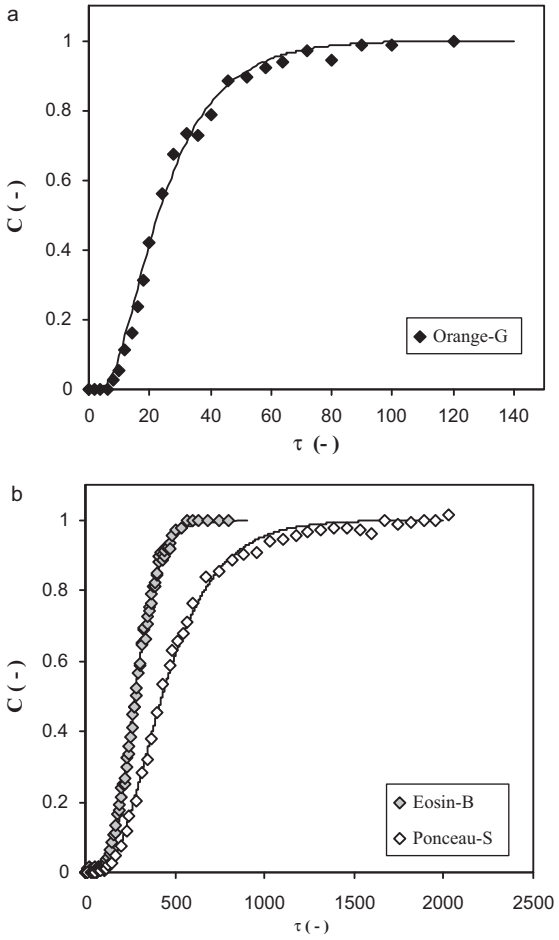

Fig. 5. Experimental and calculated breakthrough curves: (a) 2.5×10^{-4} mol/L Orange-G and (b) 2×10^{-4} mol/L Eosin-B and 1×10^{-4} mol/L Ponceau-S.

Dyes were eluted after the dispersion experiments only with demineralized water and the membrane adsorber was free of dye with 100 mL of water at room temperature. As adsorbed dye can be eluted with more than 2 L of water with high ion strength at 50 °C, the adsorption observed in the dispersion experiments is due to non-ionic adsorption.

The experimental breakthrough curves were fitted by the model assuming the infinity value of dimensionless adsorption constant and delaying the curves calculated with proper value of parameter *m*: 1, 1.3 and 4 for Orange-G, Eosin-B and Ponceau-S, respectively. The best correlation between calculated and experimental breakthrough curves was obtained with the Peclet number equal to 2.1 ± 0.1 for the three dyes. Thus, the dispersion coefficient was the same for the three dyes since it basically depends on the hydrodynamic conditions.

4.1.3. Dynamic adsorption experiments of single solutes

Fig. 5 shows the breakthrough curves in adsorbing conditions (Sartobind D) for the three dyes at the following dye concentrations: 2.5×10^{-4} mol/L Orange-G, 2×10^{-4} mol/L Eosin-B and 1×10^{-4} mol/L Ponceau-S. The saturation of the membrane adsorber, which is obtained when the outlet dimensionless concentration is equal to 1, was different for the three dyes, as it can be deduced from the equilibrium data. Thereby, the satura-

tion was observed at the dimensionless time of 110, 568 and 1750 for Orange-G, Eosin-B and Ponceau-S, respectively. In contrast, the time to reach 5% saturation (the breakthrough point) was less dependent on the dye. The breakthrough point for Orange-G was obtained at the dimensionless time of 10, while it was 132 for Eosin-B and 173 for Ponceau-S. Orange-G showed very different adsorption features from the other dyes, probably due to its lower molecular weight and molecular charge. The similarity of Eosin-B and Ponceau-S in the time taken to achieve the breakthrough point, and their divergence to reach saturation, can be explained by the different adsorption constant values.

The optimized K_{ads} parameter was obtained by fitting the experimental breakthrough curves with the model for each dye. As can be seen in Fig. 5, the breakthrough curves calculated, using the above values of the equilibrium parameters and Peclet number, simulate the experimental curves sufficiently. In all cases, the SSE was lower than 10^{-3}. The characteristic adsorption time depends on the dye and the values calculated from the optimized K_{ads} values used in the predictions are shown in Table 3. As the characteristic adsorption time for Ponceau-S is of 18.2 s, which is lower than the process time (23.6 s), adsorption is the relevant process in the overall dynamic process of this dye. The carboxylic group in Eosin-B showed a faster adsorption with the nitrogen atom of diethylamine of the Sartobind D membrane than the two sulfonic groups present in Orange-G. However, the characteristic time for the desorption process increases with the dye's molecular size and the number of functional groups.

4.2. Dynamic adsorption of binary mixtures

Binary dye mixtures were separated on a Sartobind D membrane. Fig. 6 shows the breakthrough curves for the separation of two Orange-G/Eosin-B mixtures (1×10^{-4} mol/L/1×10^{-4} mol/L and 3×10^{-4} mol/L/1×10^{-4} mol/L) and one Orange-G/Ponceau-S mixture (2.5×10^{-4} mol/L/1×10^{-4} mol/L).

There is a clear difference between the two dyes in the situation of their breakthrough curves, as it can be expected from the experimental results for the single dyes. For instance, the Eosin-B is fully adsorbed during the initial period, whereas pure Orange-G is obtained in the outlet stream of the membrane adsorber because this dye does not adsorb significantly. The dimensionless outlet Orange-G concentration was 48% and 77% of the feed concentration for Orange-G/Eosin-B mixtures when the dimensionless time was equal to 30.

The breakthrough curves of Orange-G showed overshooting and the dimensionless Orange-G concentration in the liquid-phase reached values higher than 1, since the higher adsorption of Eosin-B molecules displaced part of the adsorbed Orange-G molecules. At very high dimensionless time, the dimensionless concentration of both dyes tends to 1, thereby indicating that the membrane adsorber is saturated. In competition, the small molecule, Orange-G, will cross the membrane faster than the other dye and will occupy the diethylamine functional groups first [7].

The main difference between the breakthrough curves of the three mixtures is the dependence of overshooting on the feed Orange-G concentration. The maximum dimensionless concentration decreased and was delayed when the feed Orange-G concentration was high.

Dyes were separated in the binary mixtures during the first 25 min for the Orange-G/Eosin-B mixture, and the first 40 min for the Orange-G/Ponceau-S mixture. The breakthrough curves of each component of the mixtures were affected by the presence of the second component: (i) the maximum dimensionless outlet Orange-G concentration was 1.10 for Orange-G/Eosin-B mixture and 1.04 for Orange-G/Ponceau-S mixture; (ii) the breakthrough point was observed at 96 for Eosin-B and at 159 for Ponceau-S; (iii) the dimensionless time to saturate the membrane was 800 for Orange-G/Eosin-B and 1200 for Orange-G/Ponceau-S mixtures.

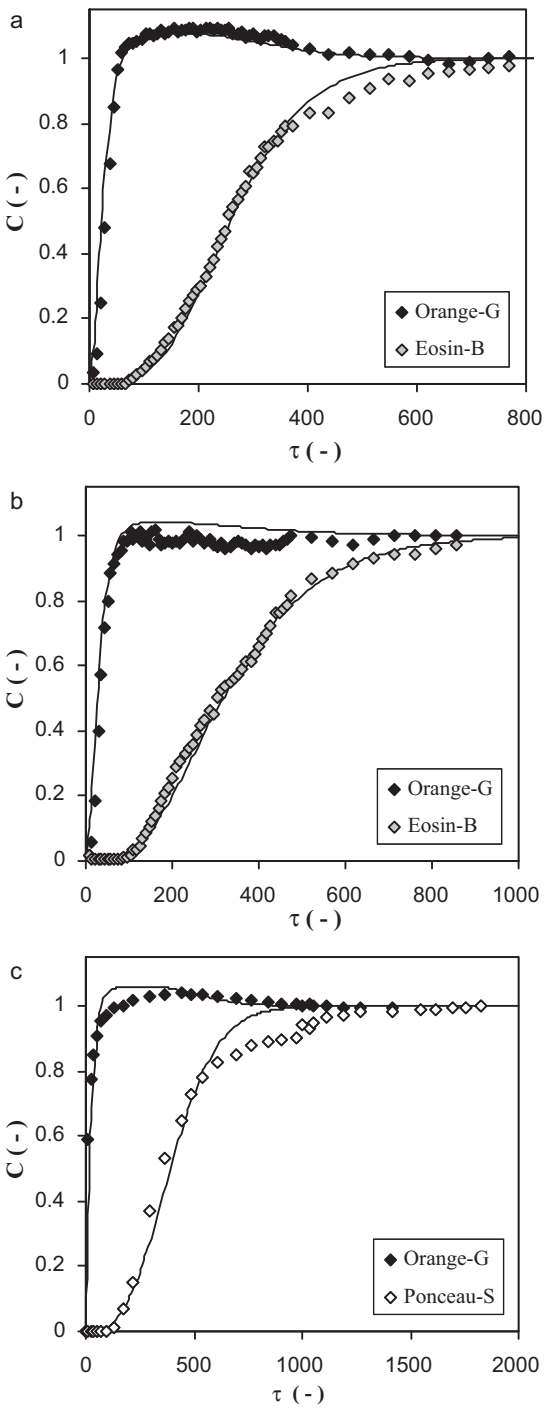

Fig. 6. Experimental and calculated breakthrough curves of binary dye mixtures: (a) 10^{-4} mol/L Orange-G/10^{-4} mol/L Eosin-B mixture, (b) 3×10^{-4} mol/L Orange-G/10^{-4} mol/L Eosin-B mixture, and (c) 2.5×10^{-4} mol/L Orange-G/1×10^{-4} mol/L Ponceau-S mixture.

Fig. 6 shows also the simulated breakthrough curves together with the experimental data. The simulations were conducted with the generalized model presented above and with the dimensionless parameters obtained in the simulation of breakthrough curves of single dyes. Satisfactory correlation was obtained for all mixtures. The simulated breakthrough curve of Orange-G in 3×10^{-4} mol/L Orange-G/1×10^{-4} mol/L Eosin-B mixture differs

from the experimental curves in the prediction of slight overshooting with dimensionless concentration values higher than 1.

5. Conclusions

A mathematical model is put forward for the description of the dynamic adsorption processes of single and binary mixtures of two anionic dyes on an ion-exchange membrane adsorber. The model was presented in terms of characteristic times for the convection, dispersion, adsorption and desorption components of the general processes. The model is based on the extended Langmuir isotherm to describe competitive adsorption in multi-component mixtures.

Single solute adsorption under equilibrium conditions for the three dyes analyzed (Orange-G, Eosin-B and Ponceau-S) is described well with the Langmuir equation. The dynamic experiments allowed the determination of the Peclet number and the dimensionless adsorption constant. The breakthrough curves of the binary mixtures were simulated satisfactorily by the parameters determined with the single-dye experiments. The breakthrough curves of Orange-G showed overshooting with a maximum concentration higher than the feed concentration, due to the higher adsorption of Eosin-B and Ponceau-S.

The separation of two anionic dyes was achieved using an ion-exchange membrane adsorber during the initial period of time when Eosin-B and Ponceau-S were fully adsorbed and pure Orange-G eluted the membrane adsorber.

Acknowledgement

The authors are grateful to the Spanish 'Ministerio de Ciencia y Tecnología' (project CTQ2009-11465) for funds received to carry out this study.

References

[1] R.K. Lewus, G. Carta, Binary protein adsorption on gel-composite ion-exchange media, AIChE J. 45 (1999) 512–522.
[2] B.J. Horstmann, H.A. Chase, Modeling the affinity adsorption of immunoglobulin-G to protein-A immobilized to agarose matrices, Chem. Eng. Res. Des. 67 (1989) 243–254.
[3] G.L. Skidmore, B.J. Horstmann, H.A. Chase, Modeling single-component protein adsorption to the cation exchanger Sepharose FF, J. Chromatogr. 498 (1990) 113–128.
[4] C. Pelekani, V.L. Snoeyink, Competitive adsorption in natural water: role of activated carbon pore size, Water Res. 33 (1999) 1209–1219.
[5] E. Lorenc-Grabowska, G. Gryglewicz, Adsorption characteristics of Congo Red on coal-based mesoporous activated carbon, Dyes Pigm. 74 (2007) 34–40.
[6] S.J. Allen, G. Mckay, J.F. Porter, Adsorption isotherm models for basic dye adsorption by peat in single and binary component systems, J. Colloid Interface Sci. 280 (2004) 322–333.
[7] B. Noroozi, G.A. Sorial, H. Bahrami, M. Arami, Adsorption of binary mixtures of cationic dyes, Dyes Pigm. 76 (2008) 784–791.
[8] K.K.H. Choy, J.F. Porter, G. Mckay, Langmuir isotherm models applied to the multicomponent sorption of acid dyes from effluent onto activated carbon, J. Chem. Eng. Data 45 (2000) 575–584.
[9] R. Ghosh, Protein separation using membrane chromatography: opportunities and challenges, J. Chromatogr. A 952 (2002) 13–27.
[10] Z. Ma, K. Masaya, S. Ramakrishna, Immobilization of Cibacron blue F3GA on electrospun polysulphone ultra-fine fiber surfaces towards developing an affinity membrane for albumin adsorption, J. Membr. Sci. 282 (2006) 237–244.
[11] S.P. Zhang, Y. Sun, Steric mass-action model for dye–ligand affinity adsorption of protein, J. Chromatogr. A 957 (2002) 89–97.
[12] T. Vicente, M.F.Q. Sousa, C. Peixoto, J.P.B. Mota, P.M. Alves, M.J.T. Carrondo, Anion-exchange chromatography for purification of rotavirus-like particles, J. Membr. Sci. 311 (2008) 270–283.
[13] M.Y. Arica, H.N. Testereci, A. Denizli, Dye-ligand and metal chelate poly(2-hydroxyethylmethacrylate) membranes for affinity separation of proteins, J. Chromatogr. A 799 (1998) 83–91.
[14] D.K. Roper, E.N. Lightfoot, Separation of biomolecules using adsorptive membranes, J. Chromatogr. A 702 (1995) 3–26.
[15] W. Guo, E. Ruckenstein, Separation and purification of horseradish peroxidase by membrane affinity chromatography, J. Membr. Sci. 211 (2003) 101–111.
[16] S.Y. Suen, M.R. Etzel, A mathematical analysis of affinity membrane bioseparations, Chem. Eng. Sci. 47 (1992) 1355–1364.
[17] W. Shi, F. Zhang, G. Zhang, Mathematical analysis of affinity membrane chromatography, J. Chromatogr. A 1081 (2005) 156–162.
[18] C. Boi, S. Dimartino, G.C. Sarti, Modelling and simulation of affinity membrane adsorption, J. Chromatogr. A 1162 (2007) 24–33.
[19] J. Labanda, J. Sabaté, J. Llorens, Modeling of the dynamic adsorption of an anionic dye through ion-exchange membrane adsorber, J. Membr. Sci. 340 (2009) 234–240.
[20] W. Hayduk, H. Laudie, Prediction of diffusion coefficients for nonelectrolytes in dilute aqueous solutions, AIChE J. 20 (1974) 611.
[21] J. Bandara, J.A. Mielczarski, J. Kiwi, 1. Molecular mechanism of surface recognition. Azo dyes degradation on Fe, Ti, and Al oxides through metal sulfonate complexes, Langmuir 15 (1999) 7670–7679.
[22] J. Madhavan, F. Grieser, M. Ashokkumar, Degradation of Orange-G by advanced oxidation processes, Ultrason. Sonochem. 17 (2010) 338–343.
[23] P. Ledlain, D. Fompeydie, Determination of equilibrium constants by derivative spectrophotometry. Application of the pK_as Eosin, Anal. Chem. 15 (1985) 2561–2563.
[24] J.F. Porter, G. McKay, K.H. Choy, The prediction of sorption from a binary mixture of acidic dyes using single- and mixed-isotherm variants of the ideal adsorbed solute theory, Chem. Eng. Sci. 54 (1999) 5863–5885.
[25] J. Wang, F. Dismer, J. Hubbuch, M. Ulbricht, Detailed analysis of membrane adsorber pore structure and protein binding by advanced microscopy, J. Membr. Sci. 320 (2008) 456–467.
[26] M. Sahimi, A.O. Imdakm, The effect of morphological disorder on hydrodynamic dispersion in flow through porous media, J. Phys. A: Math. Gen. 21 (1988) 3833–3870.